Scientific Contributions Oil & Gas, Vol. 49. No. 1, March: 295 - 310

SCIENTIFIC CONTRIBUTIONS OIL AND GAS

Testing Center for Oil and Gas
LEMIGAS

Journal Homepage:http://journal.lemigas.esdm.go.id
ISSN: 2089-3361, e-ISSN: 2541-0520

Probabilistic Thin-Bed Sandstone Reservoirs Delineation in The Montara Formation, Browse Basin, Using Stochastic Inversion and AVF-A (Intercept) Analysis

Fadhil Arhab[1] and Ignatius Sonny Winardhie[2]

[1]Geophysical Engineering Post Graduate Program, Faculty of Mining and Petroleum Engineering, Institut Teknologi Bandung
Ganesa Street No. 10, Bandung, West Java, 40132, Indonesia.

[2]Seismological Engineering and Exploration Research Group, Faculty of Mining and Petroleum Engineering,
Institut Teknologi Bandung
Ganesa Street No. 10, Bandung, West Java, 40132, Indonesia.

Corresponding author: Fadhil Arhab (arhabfadhil8@gmail.com)

Manuscript received: January 30th, 2026; Revised: February 26th, 2026
Approved: February 27th, 2026; Available online: March 19th, 2026; Published: March 20th, 2026.

ABSTRACT - In the pursuit of net zero-emission targets, restrictions on new oil and gas field discoveries have intensifies the need for enhanced reservoir characterization of secondary resources in mature fields, such as thin-bed reservoirs. However, imaging thin-bed remains challenging due to the limited vertical resolution of conventional seismic data. Advanced methodologies are therefore required to accurately delineate thin-bed sandstone reservoirs and improve reservoir prediction reliability. This study integrates seismic frequency attributes and stochastic seismic inversion to enhance vertical resolution and characterize thin-bed reservoirs within the Montara Formation, Browse Basin, offshore northwestern Australia. The workflow begins with tuning thickness analysis to identify thin-bed responses, followed by the construction of reflectivity volumes for intercept-based amplitude variation with frequency (AVF-A) analysis and seismic inversion. The results indicate that thin-bed sandstone reservoirs were predominantly deposited during the syn-rift phase and exhibit a Northeast (NE)–Southwest (SW) orientation. These reservoirs are distributed in the eastern well area of the SW region and the western well area of the NE region, with thicknesses of up to 140 m. Probabilistic inversion results indicate reservoir probabilities exceeding 50% within the target zones. These findings demonstrate that integrating seismic frequency attributes with stochastic seismic inversion provides a robust framework for thin-bed bed delineation and reservoir prediction under sub-tuning conditions

Keywords: thin-bed reservoir, AVF-A, stochastic seismic inversion, probability analysis, syn-rift depositional system.

How to cite this article:

Fadhil Arhab and Ignatius Sonny Winardhie, 2026, Probabilistic Thin-Bed Sandstone Reservoirs Delineation in The Montara Formation, Browse Basin, Using Stochastic Inversion and AVF-A (Intercept) Analysis, Scientific Contributions Oil and Gas, 49 (1) pp. 295-309. DOI org/10.29017/scog.v49i1.1997.

INTRODUCTION

The global transition towards net-zero emission targets has constrained new hydrocarbon field development, thereby increasing the importance of reservoir characterization to identify alternative accumulation sources, such as thin-bed reservoirs. Although global energy demand is projected to decline by approximately 75% by 2050 (International Energy Agency 2023), optimizing existing resources remains critical during the energy transition.

Thin-bed reservoirs are inherently difficult to image using conventional seismic techniques due to limited vertical resolution. Consequently, advanced approaches are required to enhance reservoir resolution and improve the characterization of sub-tuning reservoir. To complement the inversion analysis, frequency-domain seismic attributes are utilized to capture attenuation variations and frequency-dependent responses within the seismic signal (Han et al., 2023).

This study focuses on the Montara Formation in the Browse Basin, northwestern Australia, which comprises thin-bedded siliciclastic reservoirs that thicken toward the southeast (Figureure 1). The lithology is predominantly sandstone, sealed by the Echuca Shoals and Jamieson formations, with hydrocarbon charge sourced from the Plover Formation, which contains thin coal layers and prodelta shales.

Well data indicate that the Poseidon-2 well in the northwestern area contains gas-bearing intervals with thicknesses below the seismic tuning thickness, whereas the Pharos well in the southeastern area penetrates reservoir intervals exceeding the tuning threshold (ConocoPhillips 2011, 2012, 2015). Despite being sub-tuning in thickness, these thin beds represent viable hydrocarbon targets and therefore require accurate delineation.

Previous studies (Hosseinzadeh et al., 2025) have compared various seismic inversion methods and concluded that, despite advancements in deterministic inversion techniques, uncertainty

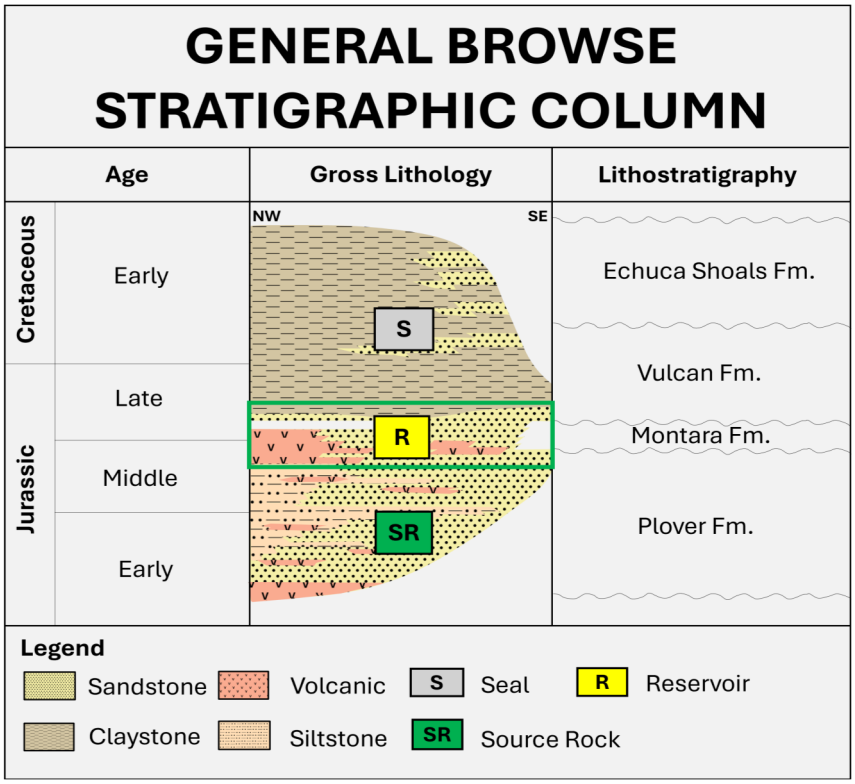

Figure 1. Stratigraphic column of Browse Basin (ConocoPhillips 2012). The Montara formation is predominantly composed of thin sandstone layers that thicken toward the southeast, as indicated by the green box.

quantification and the resolution of thin reservoirs remain significant challenges. Accordingly, this study has three objectives remain significant challenges. Accordingly, this study has three primary objectives: (i) to determine the spatial distribution of sensitive elastic parameters within the thin-bed target zone using stochastic seismic inversion and seismic frequency attributes, (ii) to evaluate the probability and thickness distribution of thin-bed reservoirs, and (iii) to interpret the depositional environment, geological structures, and petroleum system associated with the thin-bed target zone.

The novelty of this study lies in demonstrating how the integration of stochastic seismic inversion and intercept-based amplitude variation with frequency (AVF-A) attributes can effectively delineate thin-bed sandstone reservoir and improve reservoir prediction in areas where conventional deterministic inversion and limited petrophysical data provide insufficient constraints.

METHODOLOGY

Data

This study utilizes seismic data acquired in the Browse Basin, offshore Western Australia, together with supporting well logs and well reports. The seismic dataset covers Inline 2300 - 3400 and Xline 1300 – 2800. The available volumes consist of preserved partial-angle stacks (near: 6 - 18°C, mid: 18 - 30°C, far: 30 - 42°C) for elastic inversion and a non-preserved post-stack volume for horizon interpretation, sampled at 4 ms.

Six wells – Proteus, Kronos, Boreas, Poseidon 1, Poseidon 2, and Pharos – were incorporated in this study. Within the Montara Formation, the available well logs include gamma ray (GR), deep (RD) & shallow (RS) resistivity, neutron porosity (NPHI), bulk density (RHOB), acoustic impedance (AI) and the Vp/Vs ratio derived from P-wave and S-wave velocities (Figure. 2). Well reports were incorporated to establish formation markers, which

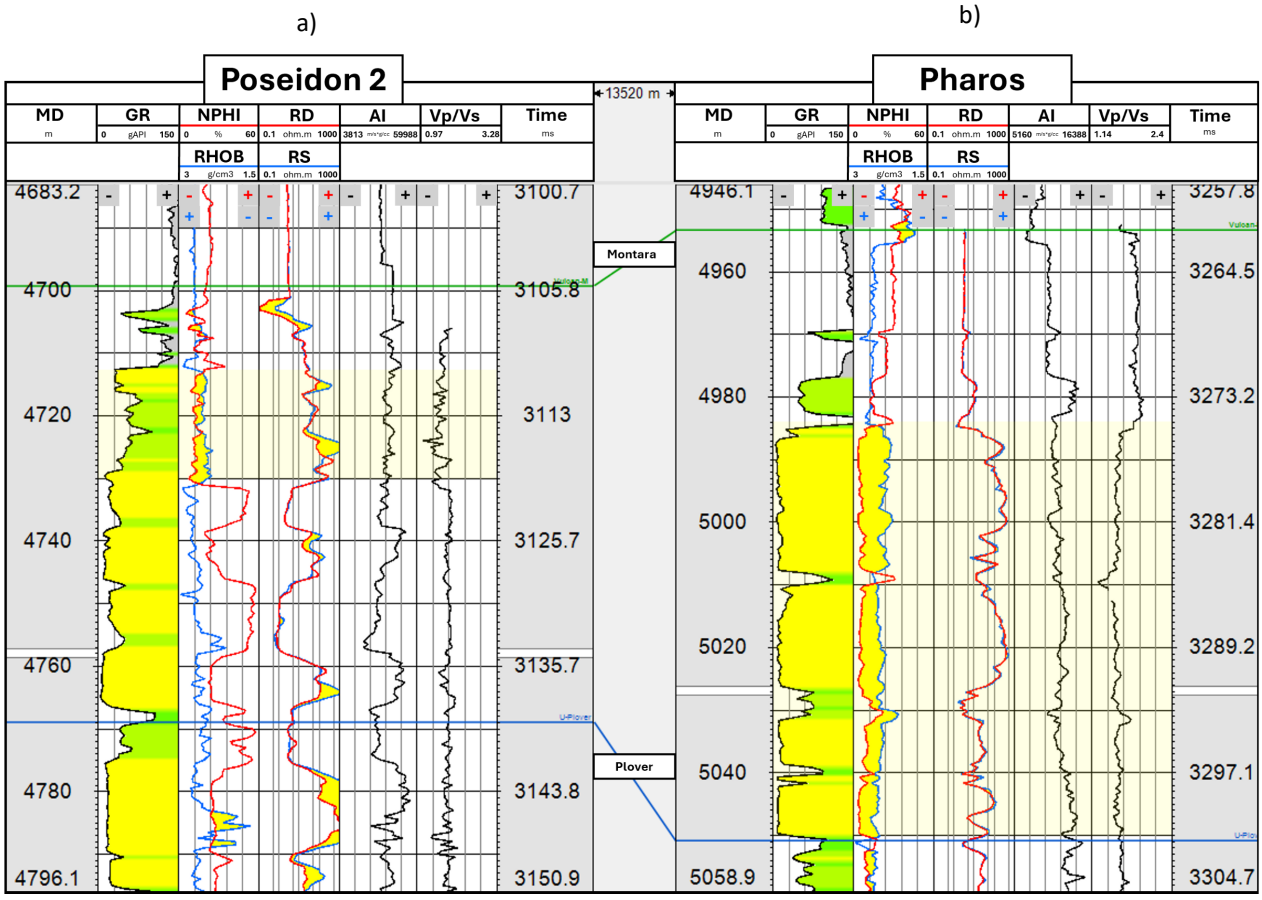

Figure 2. Well correlation from northwest (NW) to southeast (SE) wells: a). Poseidon 2 and b). Pharos. Hydrocarbon reservoir indications are characterized by low GR log, a cross-over between NPHI and RHOB logs, and increased resistivity log responses, as highlighted by the yellow blocks.

were subsequently refined through well-log correlation and seismic horizon interpretation across the Montara interval.

A tuning thickness analysis was conducted to evaluate the distribution of reservoir net sand within the Montara Formation in the well area using seismic data. The analysis focused on intervals characterized by decreasing GR values, NPHI–RHOB crossover, increasing resistivity, and a decreasing Vp/Vs. The results reveal limitations in seismic resolution for imaging thin-bed reservoirs as (Table I), particularly in the vicinity of the northwestern wells.

Time-depth conversion

Time–depth conversion was performed using the layer-cake method due to its suitability for depth conversion in geologically complex settings. This approach converts seismic horizons into the depth domain by sequentially stacking velocity layers, analogous to the layering a cake. A velocity model constructed from checkshot data was applied, and the Montara Formation was subdivided into 20 zones using a moving-average technique to improve depth-conversion accuracy.

Reflectivity

Prior to generating the reflectivity volumes, the partial-angle stacks were subjected to amplitude spectrum bandwidth equalization using the near-angle stack as the reference. This process, commonly referred to as bandwidth matching, applies a bandpass-type filter defined by low-cut, low-pass, high-pass, and high-cut parameters.

The near-angle stack was selected as the reference because it typically exhibits the broadest bandwidth due to shorter propagation paths and reduced frequency attenuation. Consequently, it provides superior spectral content and overall seismic quality compared to mid- and fa-angle stacks.

According to Hutabarat et al. (2014), AVO inversion can derive elastic attributes such as Vp, Vs, and density, which may subsequently serve as direct hydrocarbon indicators, including the Vp/Vs ratio. In this study, reflectivity volumes for P-wave velocity (R_P) and Vp/Vs $\left(R_{Vp/Vs}\right)$ were generated using the hierarchical Bayesian AVO facies inversion approach proposed by Grana et al. (2025), as expressed in Equation 1, 2, and 3.

This method enables simultaneous elastic parameter estimation and facies classification within a consistent parameter space defined by acoustic impedanc (AI) and Vp/Vs. The parameter k, representing the wet-trend slope, was estimated from the Pharos well and has a value of 0.58.

$$A_1(\theta) = \frac{1}{2} - \frac{2}{5}tan^2(\theta) - \frac{18}{5}k^2sin^2(\theta) \quad (1)$$

$$\mathrm{A_2(\theta) = 4k^2sin^2(\theta)} \quad (2)$$

$$\begin{bmatrix} R(\theta_1) \\ R(\theta_2) \\ R(\theta_3) \end{bmatrix} = \begin{bmatrix} A_1(\theta_1) & A_2(\theta_1) \\ A_1(\theta_2) & A_2(\theta_2) \\ A_1(\theta_3) & A_2(\theta_3) \end{bmatrix} \begin{bmatrix} R_P \\ R_{VpVs} \end{bmatrix} \quad (3)$$

In Equations 1 through 3, $??(??_{1,2,3})$ denotes the seismic partial-angle stacks (near, mid, far), k represents the quadratic Vs-to-Vp ratio coefficient, and (R_P) and $R_{Vp/Vs}$ correspond to P-wave velocity and Vp/Vs reflectivity volumes, respectively (Grana et al., 2025) .

Table 1. Tuning thickness analysis.

Formation	Well	Thickness (m)	Wavelet length (ms)	Dominant seismic frequency (Hz)	Tuning thickness limit (m)	Seismic resolution
Montara	Boreas	34	114.730	35	38.434	Not resolved
	Kronos	14			36.760	Not resolved
	Pharos	65			31.157	Resolved
	Poseidon 2	17			34.298	Not resolved
	Proteus	92			35.210	Resolved

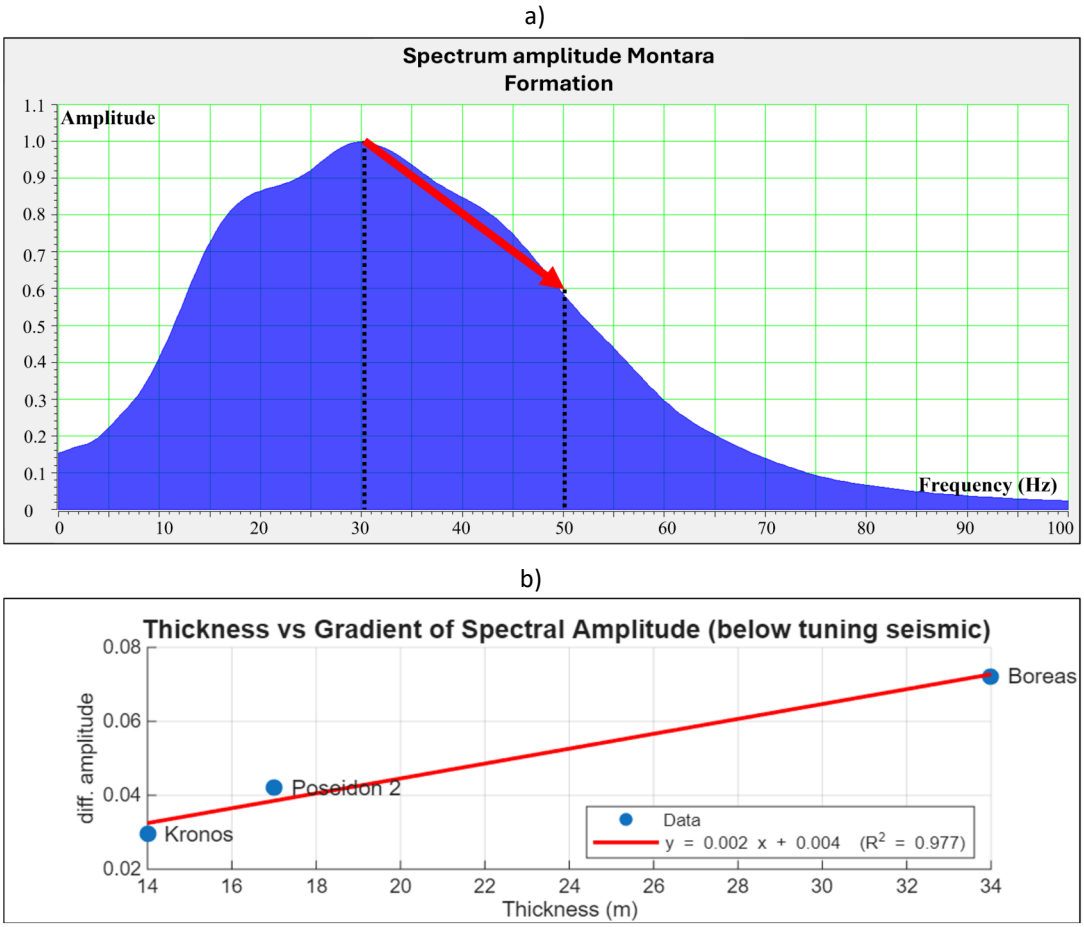

Figure 3. Identification of reservoir lithology in frequency domain: a). Amplitude decay, b). Correlation thickness to frequency. The strong correlation between the spectral amplitude gradient and thickness suggests a clear relationship between the frequency domain response and bed thickness.

Seismic frequency attribute

In the delineation of thin-bed reservoirs, frequency-domain seismic attributes are employed to enhance specific characteristics of the seismic signal. Thin-bed thickness controls the interference pattern of reflected seismic waves, resulting in periodic spectral notches and selective frequency attenuation within the seismic amplitude spectrum (Partyka et al., 1999).

Spectral decomposition

Spectral decomposition was conducted prior to the amplitude variation with frequency (AVF) analysis by extracting low-, mid-, and high-frequency components of 30, 40, and 50 Hz, respectively (Figure. 3a). Variations in thin-bed thickness correlate with changes in the spectral amplitude gradient (Figure. 3b). This technique transforms seismic data from the time domain into the frequency domain, separating the seismic volume into constant-frequency components, allowing each frequency band to be analyzed independently, without relying on the stationarity assumptions inherent in conventional Fourier transforms (Mandong et al., 2021).

In this study, spectral decomposition was conducted using the Continuous Wavelet Transform (CWT) with a Ricker wavelet, as shown in Equation 4. The CWT applies wavelets of varying frequencies and window lengths to the seismic signal, enabling improved resolution characterized by thinner anomalies, more focused reflection events, and reduced tuning effects (Haris et al., 2017). (4)

$$W(\alpha,\tau) = \frac{1}{\sqrt{a}}\int_{-\infty}^{\infty} S(t)\Psi * \left(\frac{t-\tau}{a}\right) dt \qquad (4)$$

where $S(t)$ is seismic amplitude, Ψ is wavelet function, t is time (s), τ is time the shift (s), and is wavelet scaling factor (Sinha et al., 2005).

Amplitude variation with frequency (AVF)

Subsequently, reflectivity volumes derived from the spectral decomposition were grouped into frequency gathers to analyze frequency-dependent amplitude decay associated with seismic attenuation in gas-bearing zones.

The grouped frequency volumes were analyzed using the two-term Aki–Richards approximation to derive intercept and gradient attributes, as expressed in Equation (5). The AVF attribute calculation incorporates:

- A start frequency, defined as the dominant frequency obtained from the spectral decomposition, and
- An end point, determined based on the amplitude decay trend (amplitude spectrum shape).

$$y = I + (Gsin^2x)(5) \quad (5)$$

In this formulation, y represents spectrum, I denotes the intercept, G represents the gradient, and x corresponds to seismic frequency.

Seismic inversion

Deterministic

A deterministic inversion was first performed using the Linear Programming Sparse Spike (LPSS) method on the selected sensitive parameters. The resulting horizontal variogram models were used as input for the stochastic inversion.

The LPSS method estimates acoustic impedance (AI) from sparse reflectivity while incorporating the effects of the low-frequency model (LFM) near the well control. The inversion parameters included 20% sparseness, a maximum cut-off frequency of 10 Hz, a window length of 128 samples, and a scaling factor of 0.1. The method employs linear programming to minimize the least absolute deviation objective function.

The deterministic inversion generated horizontal variogram parameters for AI and Vp/Vs, with range values of 7.548 m (AI) and 6.968 m (AI), with sill values of 68.195 m (AI) and 7.21 (Vp/Vs), and nugget values of 0 for both parameters.

Stochastic

Subsequently, stochastic seismic inversion was performed using a geostatistical approach. This method requires a low-frequency model (LFM) and horizontal variograms derived from the deterministic seismic inversion. The incorporation of geostatistical analysis improves reservoir characterization by addressing limitations in lateral resolution (Handoyo et al., 2025).

A total of 20 realizations were generated for each elastic parameter, resulting in multiple equiprobable reservoir models. The workflow began with the construction of an initial stochastic model across the Montara Formation, using a mean layer thickness of 2 ms.

The inversion parameters were defined as follows: LFM standard deviation of 20%, reflectivity uncertainty of 10%, and well-data uncertainty of 5%. Horizontal variogram parameters derived from the deterministic inversion were then incorporated, along with adjustments to the vertical variogram model (Figure. 4).

RESULT AND DISCUSSION

Geological analysis

The depth structure map of the Montara Formation (Figure. 5a) indicates that structurally high areas are predominantly located in the western part of the study area, particularly around the Poseidon-1, Poseidon-2, Boreas, and Kronos wells. In contrast, structurally low areas characterized by erosional features are observed in the northwestern sector, bounded by inversion-related fault structures.

The dominant fault system trends Northeast (NE) to Southwest (SW) and exhibits a geometry that forms closed closures in the eastern area around the Pharos and Proteus wells, thereby facilitating hydrocarbon gas migration and

a)

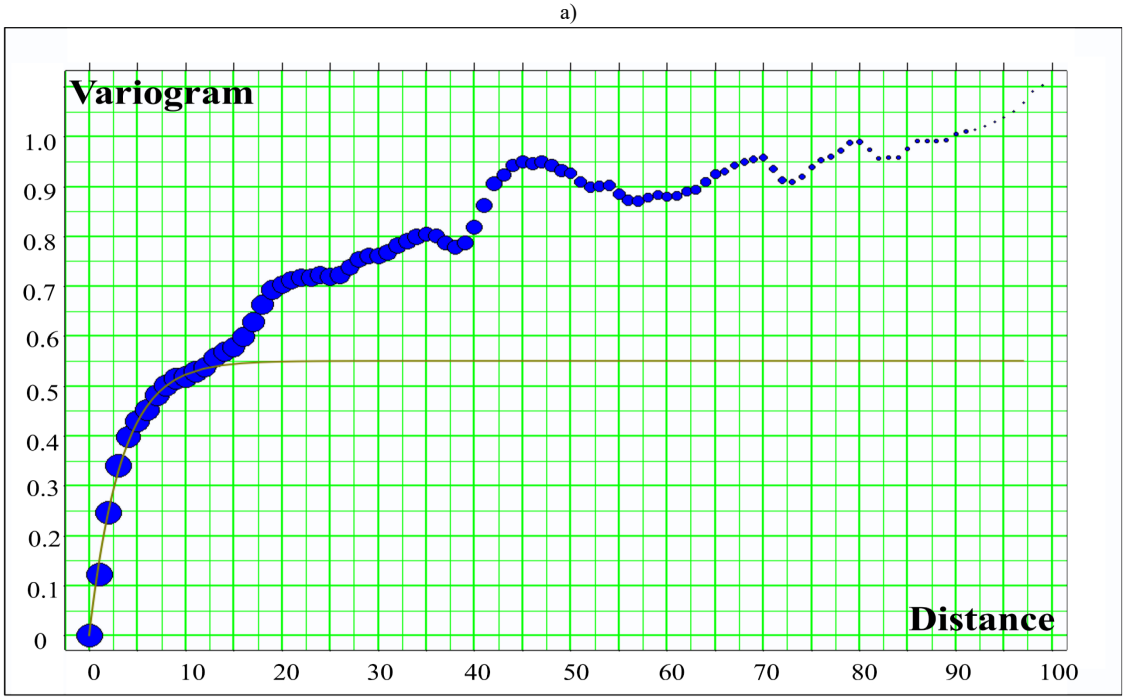

b)

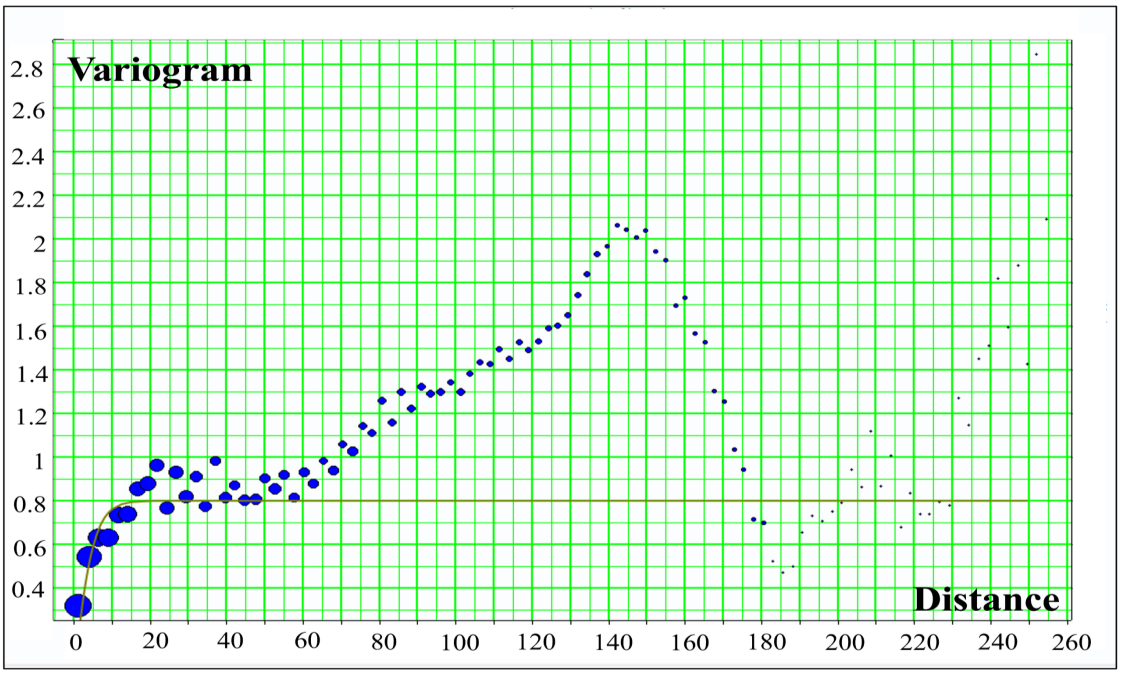

Figure 4. Vertical variogram of stochastic inversion; a). AI, b). Vp/Vs. The variogram represents the vertical continuity of elastic properties, reflecting depositional control on reservoir lithology.

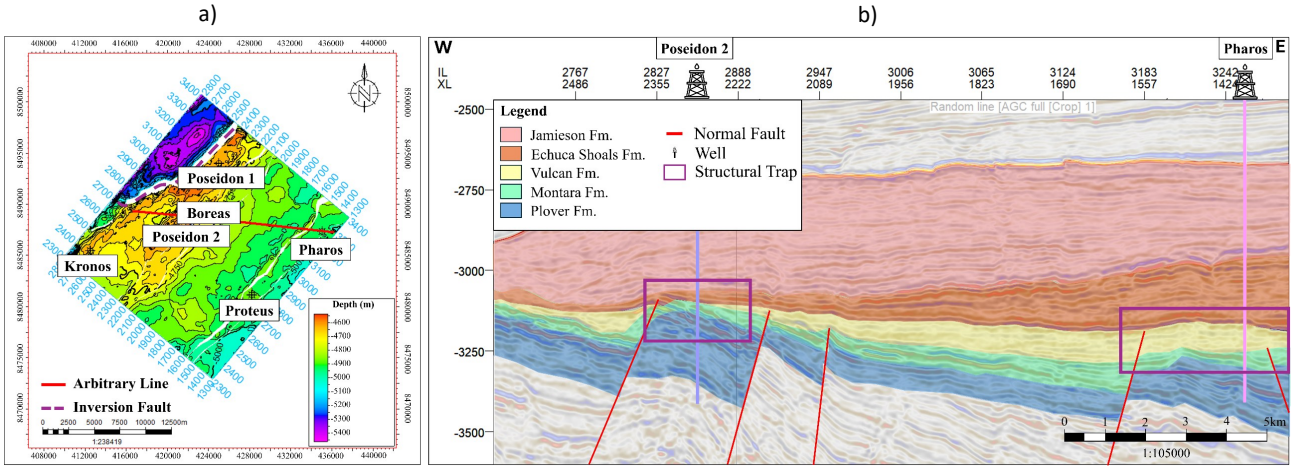

Figure 5. Geological analysis; a) Time-depth conversion slice of Montara formation, b). Seismic section. A slice from the time–depth conversion of the Montara horizon was generated to illustrate the structural elevation, which is confirmed by the seismic section along the red line.

entrapment. These structural characteristics are associated with the tectonic ofthe Montara Formation, which developed during the post-rift phase and was influenced by volcanic activity, potentially contributing to lozalized reductions in reservoir quality (ConocoPhillips 2012).

Hydrocarbon accumulations within the Montara Formation are interpreted to be hosted in structural traps, including rotated fault blocks at the Poseidon -2 well and rollover anticlines associated with inversion-related structural highs at the Pharos well (Figure. 5b). According to Setiawan et al. (2021), hydrocarbon accumulation potential is commonly associated with tectonically uplifted structural highs, which enhance trap formation at relatively shallow depths. Sealing is provided by an intraformational seal between the Montara Formation and the overlying unit. The dominant play type is interpreted as syn-rift shallow marine sandstone, characterised by thin-bedded reflections with gradually increasing amplitudes and wedge-shaped geometries that thicken toward the faults. Hydrocarbon charge into the Montara Formation is interpreted to have been sourced primarily from underlying syn-rift Jurassic source rocks of the Plover formation. Migration was likely facilitated by reactivated extensional faults during post-rift and inversion phases (Kennard et al., 2004; Geoscience Australia, 2017; Palu et al., 2017).

AVF-A (Intercept)

Based on the AVF-A slice through the Montara Formation, high-value anomalies trend NE-SW and are predominantly distributed around the northwestern (NW) well area (Figure. 6a). On the arbitrary seismic section (Figure. 6b), elevated AVF-A values follow the structural conFigureuration of the Montara Formation, particularly in zones affected by fault-related elevation changes. This finding is consistent with Han et al. (2023), who demonstrated that AVF-A responses are structurally controlled. Higher AVF-A values indicate stronger impedance contrasts, as the AVF-A attributes represents the amplitude baseline primarily governed by impedance contrasts and lithological variations. In this context, AVF-A serves as a reservoir lithology indicator based on frequency-dependent amplitude decay associated with gas-bearing reservoirs, thereby complementing the reservoir analysis from a frequency-domain perspective.

Seismic inversion

Sensitivity parameter analysis

The elastic parameters identified as most sensitive for mapping hydrocarbon-bearing reservoir lithology within the Montara Formation target zone in wells (Proteus, Kronos, Boreas, Poseidon 2, and Pharos) are acoustic impedance (AI) and Vp/Vs. Crossplot analysis (Figure. 7) indicates that reservoir sand distribution can be delineated using a low gamma-ray (GR) color key, characterized by Vp/Vs values < 1.8 and AI values > 10,000 m/s·g/cc. A low gamma ray response is indicative of sand-prone reservoir facies.

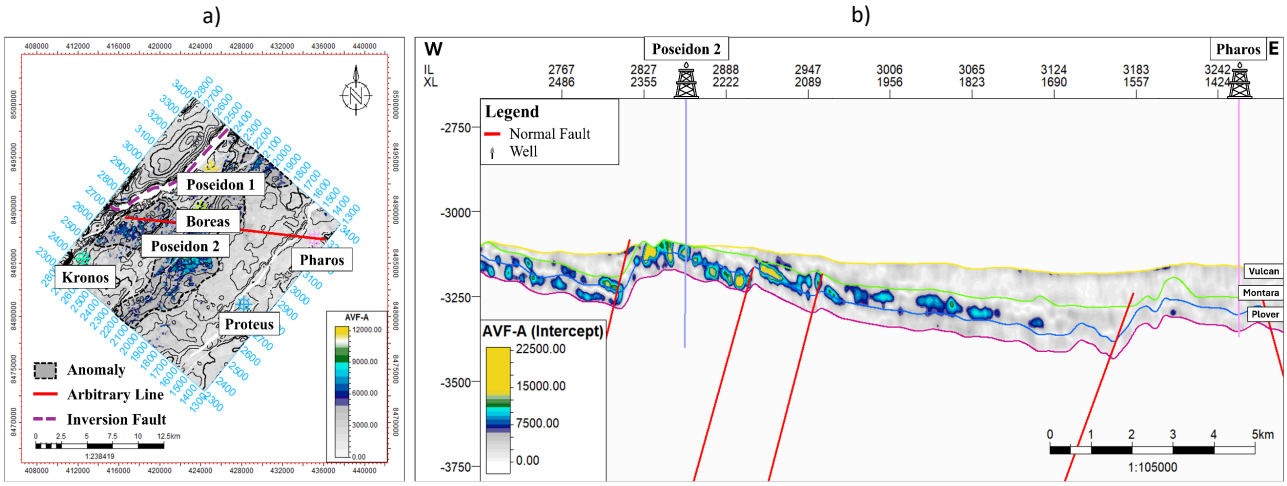

Figure 6. AVF-A; a). Slice of Montara formation, b). Seismic section. A slice from the AVF-A attribute of the Montara horizon was generated to illustrate the attribute distribution,which is confirmed by the seismic section along the red line.

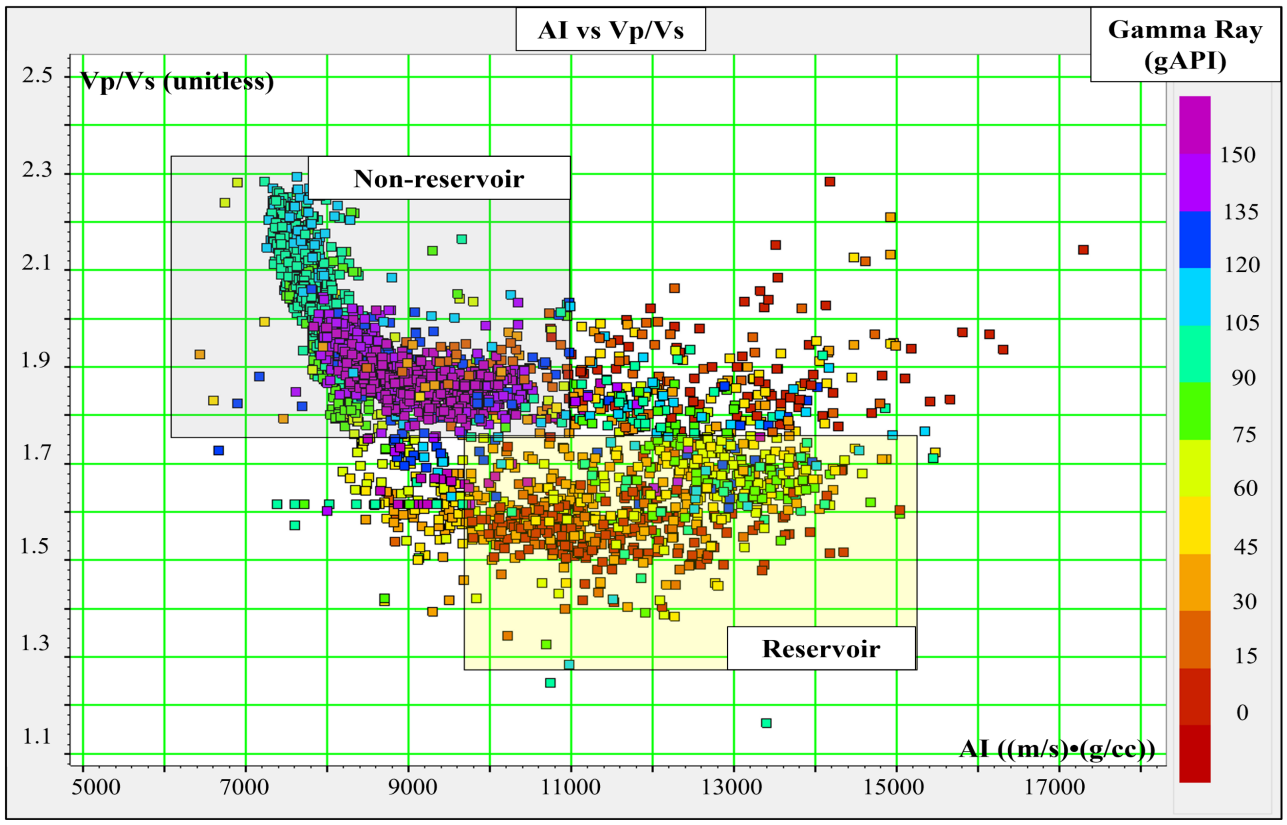

Figure 7. Sensitivity analysis of hydrocarbon reservoir's lithology. The reservoir lithology is indicated by relatively low GR readings, highlighted by the yellow box.

a)

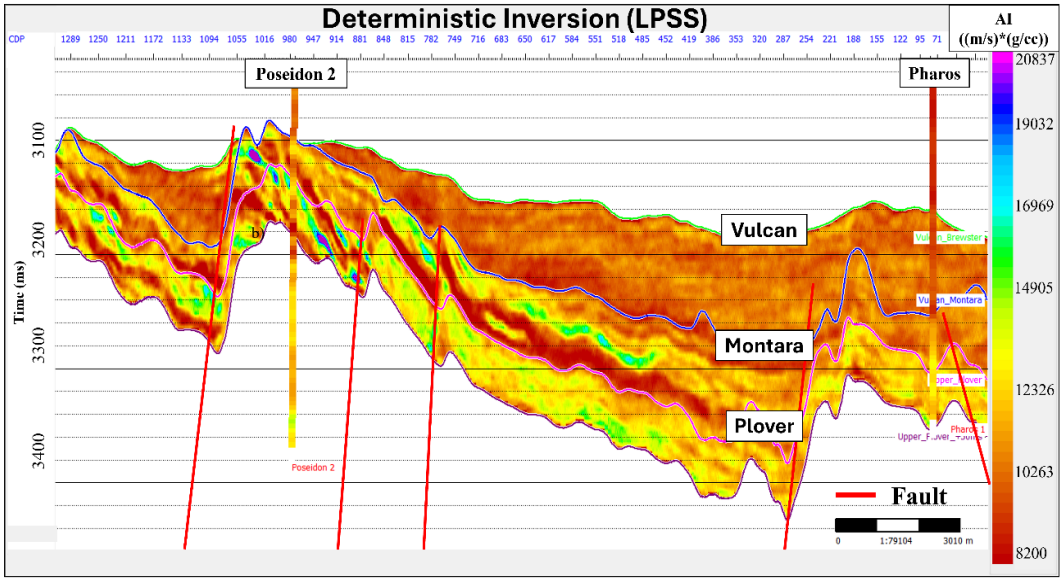

b)

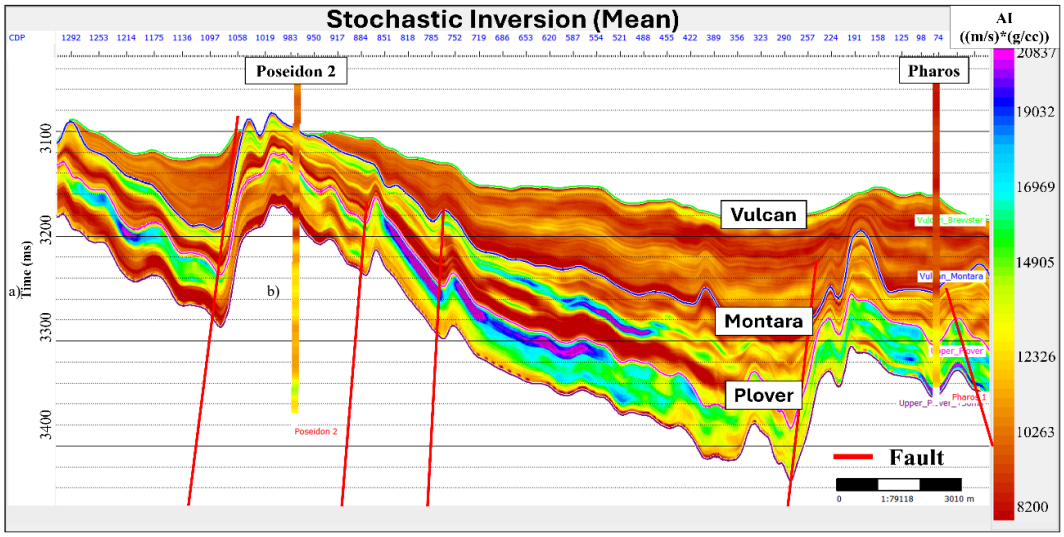

c)

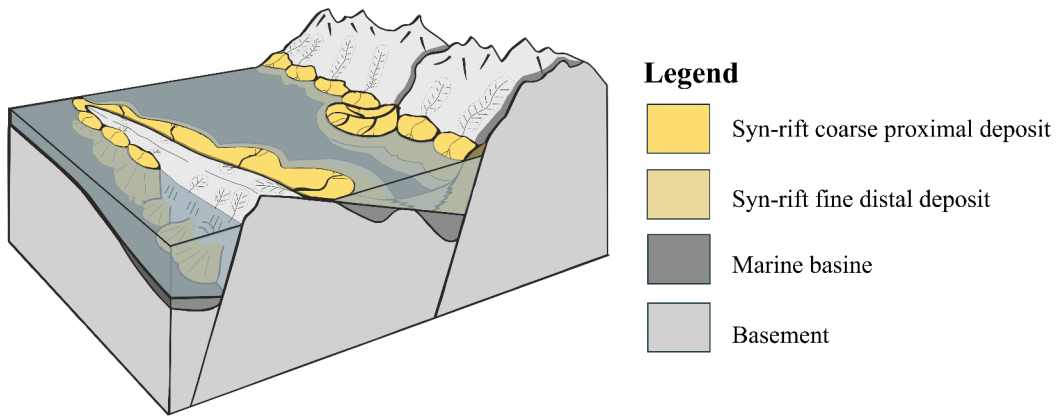

Figure 8. Seismic inversion; a). Deterministic of AI, b). Stochastic of AI, c). Geology model related to arbitrary line (redrawn after Gawthorpe and Leeder, 2000). The comparison between stochastic and deterministic inversion enables clearer delineation of syn-rift thinly deposited layers, where higher AI values are associated with sand layers characterized by a denser matrix.

For more comprehensive reservoir characterization, additional petrophysical logs such as water saturation (SW) and effective porosity (PHIE) should be incorporated. These logs enable hydrocarbon discrimination using trigonometric-based elastic attributes, including Curved Pseudo Elastic Impedance (CPEI) and Pseudo Elastic Impedance–Lithology (PEI-L).

The sensitivity of AI dan Vp/Vs is also influenced by the stratigraphic position of the Montara Formation as a thin, secondary Jurassic reservoir with localized distribution. Furthermore, poor reservoir quality sands and limited pressure communication within Jurassic intervals of the Browse Basin (Geoscience Australia 2022). These conditions suggest that Montara sandstones may locally undergo significant compaction and cementation, resulting in elevated AI values despite low GR responses. High AI AI values therefore indicate sandstone reservoirs with a relative dense matrix (Butar-Butar et al., 2023).

Based on these observations, the derived cut-off parameter values for AI and Vp/Vs were used to construct a probability model representing net sand reservoirs distribution within the Montara Formation.

Stochastic

Vertical variogram analysis of the AI and Vp/Vs (Figure 4) reveals constrasting vertical contiuity characteristics. The AI variogram exhibits an increasing semivariance pattern, indicating strong vertical continuity of lithological properties and relatively consistent sandstone deposition within individual fault blocks. This pattern is characteristic of syn-rift depositional systems, where sedimentary architecture within fault-bounded blocks may remain vertically coherent despite active extensional tectonics. In contrast, the Vp/Vs variogram displays a more complex pattern with trends cyclicity, suggesting higher vertical heterogeneity. This complexity likely reflects repeated variations in elastic properties, associated with episodic sedimentation, facies variability, and fluid changes typical in syn-rift depositional environments. The stochastic inversion results demonstrate that AI delineates reservoir sand lithology and syn-rift depositional patterns more effectively than deterministic inversion (Figure 8). This improvement reflects the ability of stochastic inversion to capture finer-scale variations associated with higher-frequency content, thereby reducing interpretational ambiguity.

Reservoir sands are identified within an AI range exceeding 10,000 m/s·g/cc and display a systematic thickening trend toward the fault (Figure 8). This thickening pattern implies the development of coarse-grained proximal deposits during the syn-rift phase adjacent to active fault zones. The geometry is controlled by normal fault systems forming rotated fault blocks.

This interpretation is consistent with the syn-rift depositional model proposed by Gawthorpe and Leeder (2000), in which sedimentation in syn-rift settings occurs contemporaneously with active extensional deformation. In such settings, stratigraphic thickness and facies distribution are strongly controlled by fault activity through: creation of accommodation space by normal fault activation; fault segmentation and linkage, producing lateral heterogeneous in reservoir thickness; and episodic fault slip that drives cyclic sedimentation, leading to thin-bedded stacking patterns.

The thin-bed stacking pattern is supported by rapid lateral variations in elastic properties (Figure 8) and a NE–SW oriented thickening trend (Figure 9). The distribution is concentrated in the eastern area relative to wells in the southwestern region and in the western area relative to wells in the northeastern region.

In the stochastic inversion mean model, relatively high AI values (> 10,000 m/s·g/cc) coincide with low Vp/Vs values (<1.8), supporting the interpretation of compact sandstone reservoir geometry.

Probability analysis based on AI and Vp/Vs cut-offs indicate a high likelihood of sand reservoir presence, with higher probabilities exceeding 50% in the eastern area of wells in the NW region and the western area of wells in the SE region (Figure 10).

a)

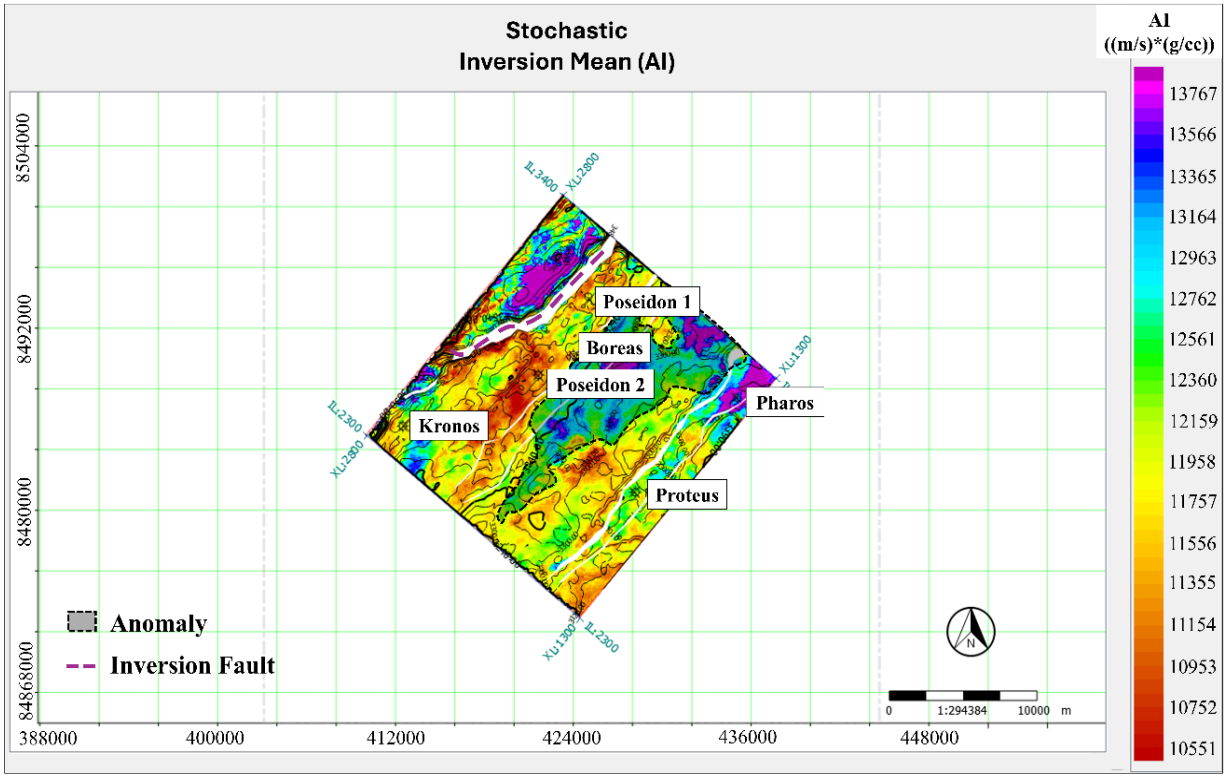

b)

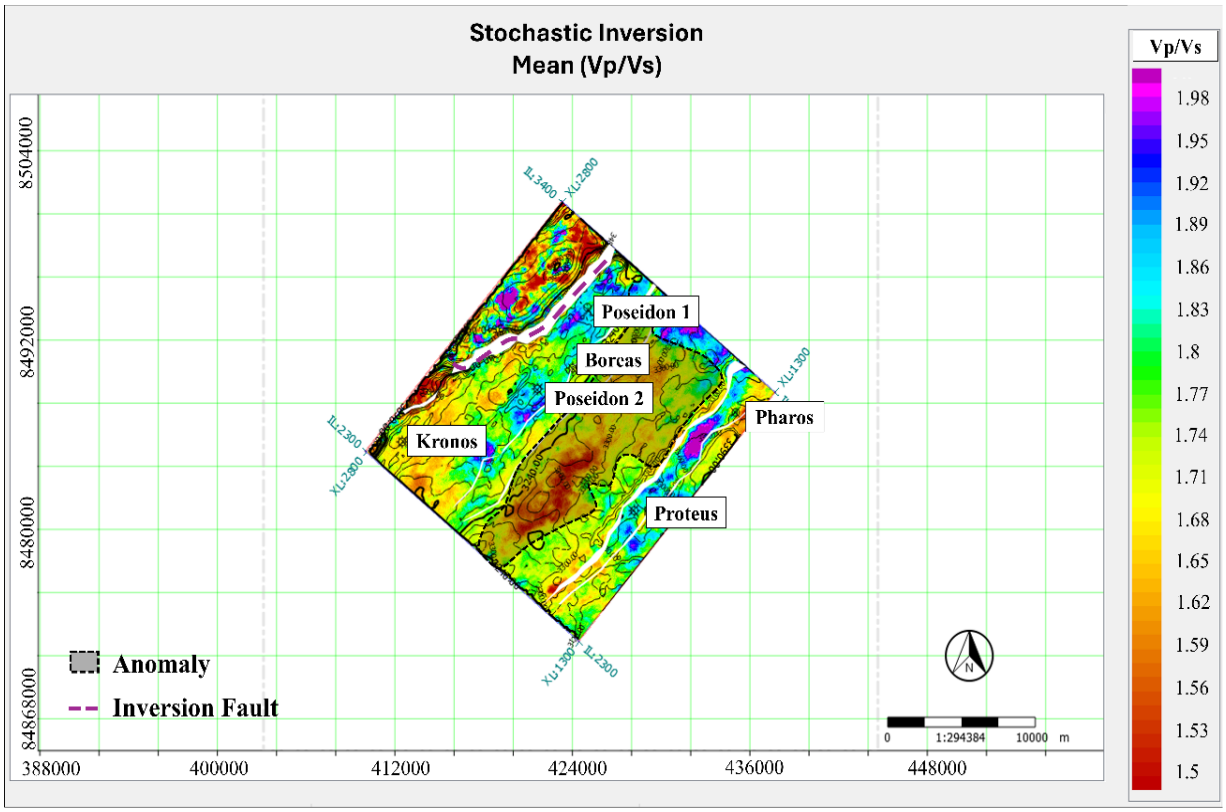

Figure 9. Stochastic inversion slices; a). AI, b). Vp/Vs. The mean stochastic inversion of AI and Vp/Vs shows dominant anomalies trending NE–SW, highlighted by shaded areas.

a)

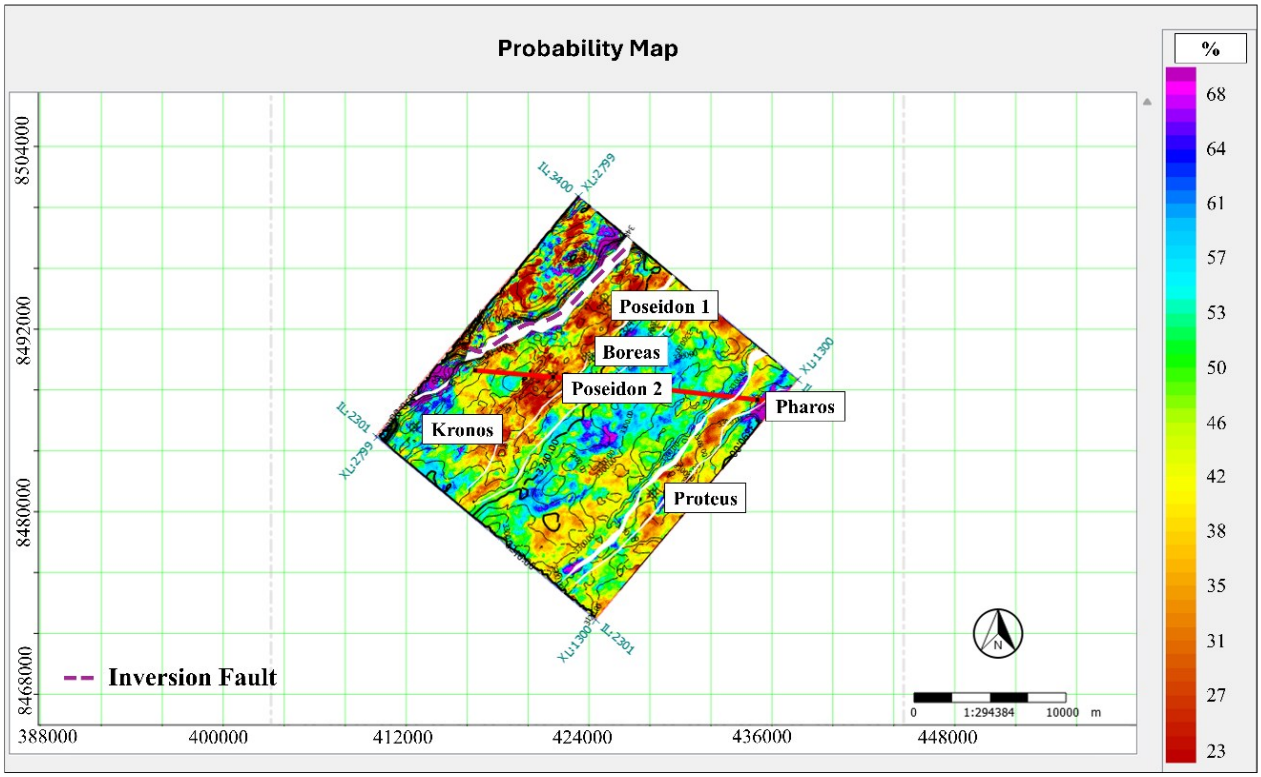

b)

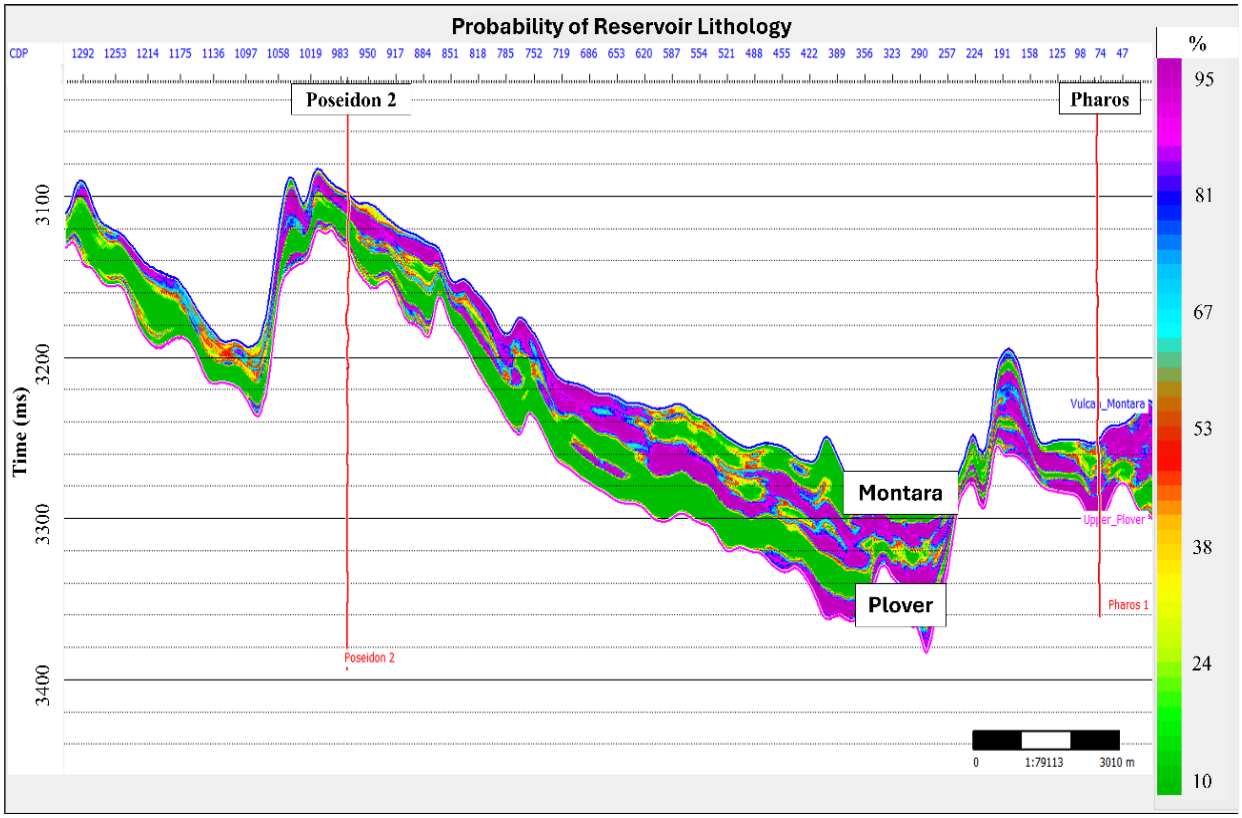

Figure 10. Stochastic inversion probability; a). Slice of Montara formation, b). Seismic section. Probability analysis based on AI and Vp/Vs cut-offs indicates a high likelihood of sand reservoirs, with probabilities exceeding 50% in the eastern area of the NW wells and the western area of the SE wells.

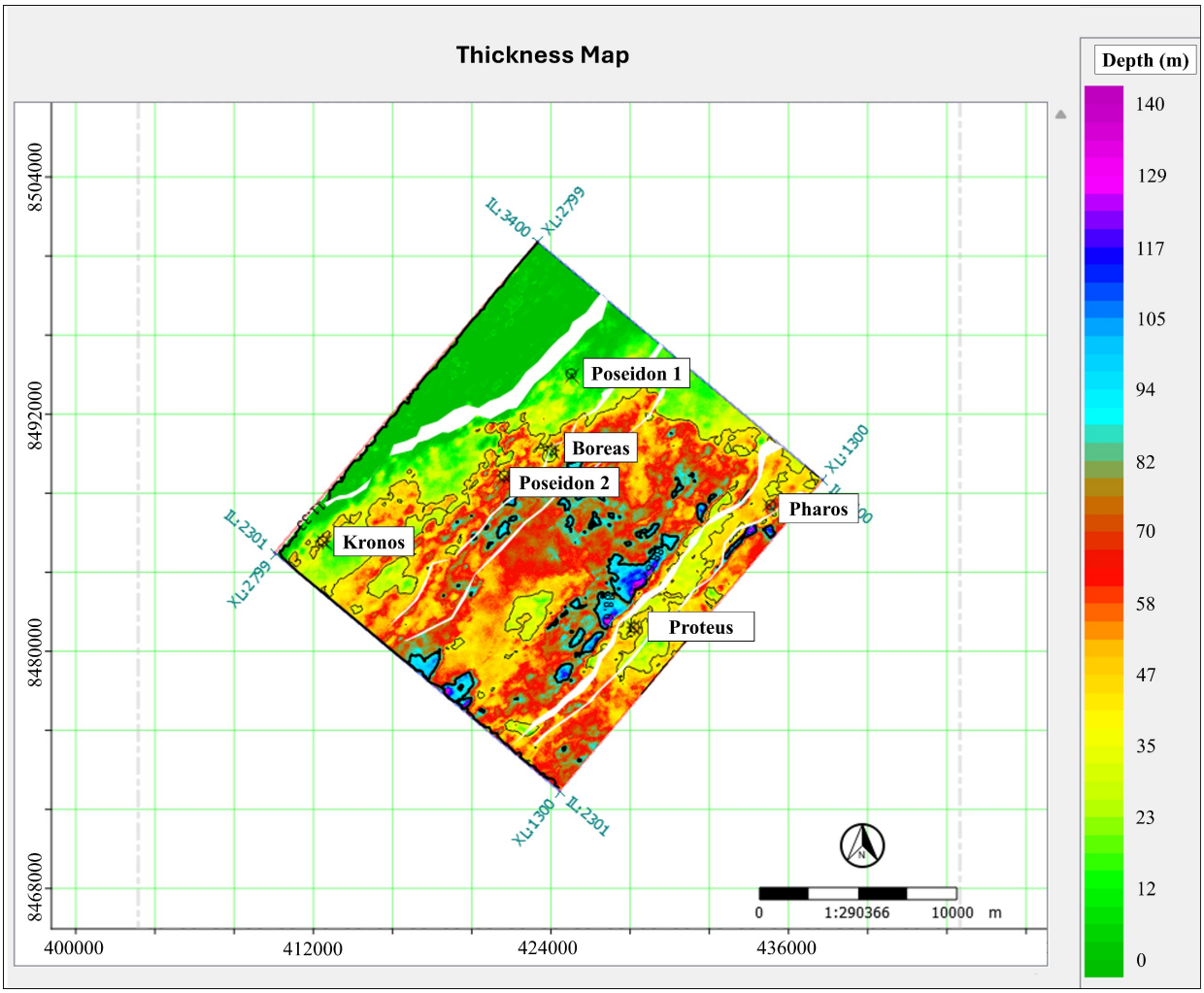

Figure 11. Thin-bed sandstone reservoir thickness.
It represents the reservoir lithology thickness at the Montara formation.

Probability estimates were derived from all of stochastic realizations, with only values within the defined sensitive parameter ranges retained. Thickness maps were subsequently generated by multiplying the depth-interval thickness by the corresponding probability values. The resulting map indicates that delineated sand reservoir reach thickness a thickness of up to 140 m (Figure 11).

This study provides a significant contribution to the delineation of thin-bed sandstone reservoir through the integration of stochastic seismic inversion and seismic frequency attributes, particularly the intercept of amplitude variation with frequency (AVF-A).

The spatial distribution of sensitive elastic parameters indicates that thin-bed sandstone reservoir within the Montara Formation is characterized by acaustic impedance (AI) values exceeding 10,000 m/s·g/cc and Vp/Vs values lower than 1.8, and are further associated with elevated AVF-A responses.

Probability analysis suggest that the likelihood of thin-bed sand reservoir occurrence exceeds 50%, with estimated thickness reaching up to 140 m. The application of the integrated methodology effectively delineates trapping geometries, including rotated fault blocks in the northwestern area and rollover anticlines associated with inversion-related structural highs in the southeastern area.

The reservoirs are interpreted as syn-rift shallow -marine sandstones with syn-rift shallow marine sandstone exhibiting a NE–SW thickening pattern toward faults. This distribution is supported by

intraformational sealing and hydrocarbon charge from underlying Jurassic Plover formation source rocks, with migration facilitated by reactivated extensional faults during post-rift and inversion phases.

SWt	Water saturation log	0.Sw
PHIt	Porosity log	%
CPEI	Curved pseudo elastic impedance	unitless
PEIL	Pseudo elastic impedance lithology	unitless

ACKNOWLDEGEMENT

The Authors gratefully acknowledge GEOScience Australia, Occam Technology, and ConocoPhillips for providing the seismic data, well data, and well reports from Browse Basin, Australia, for research purposes. The authors also express sincere appreciation to Ignatius Sonny Winardhie, the co-author, for his substantial contribution as research supervisor, providing scientific guidance throughout the study. All Figureures were generated using HRS, petrel, and MATLAB software.

GLOSSARY OF TERMS AND SYMBOLS

Terms & Symbols	Definition	Unit
AVF-A	Intercept of amplitude variation with frequency	unitless
GR	Gamma ray	gAPI
RD	Deep resistivity	ohm-m
RS	Shallow resistivity	ohm-m
NPHI	Neutron porosity	%
RHOB	Density	g/cm³
AI	Acoustic impedance	m/s·g/cc
Vp	P-wave velocity	m/s
Vs	S-wave velocity	m/s
AVO	Amplitude variation with offset	unitless
CWT	Continous wavelet transform	unitless
LPSS	Linear programming sparse spike	unitless
LFM	Low frequency model	unitless
NE	Northeast	unitless
SW	Southwest	unitless
NW	Northwest	unitless
SE	Southeast	unitless

REFERENCES

Butar, M. H. P. B., Juventa, & Marlinda, L., (2023), Identifikasi Prospek Reservoir Hidrokarbon Menggunakan Inversi Impedansi Akustik pada Blok Kampar, Lembaran Publikasi Minyak dan Gas Bumi, vol. 57, no. 1, pp. 45 – 61. https://doi.org/10.29017/ LPMGB.57.1.1324.

ConocoPhillips Pty Ltd., (2011), Poseidon-2 Well Completion Report Volume 2: Interpretive Data, National Offshore Petroleum Information Management System (NOPIMS), Australia.

ConocoPhillips Pty Ltd., (2012, 2009) Poseidon 3D Marine Surface Seismic Survey – Interpretation Report, Australia.

ConocoPhillips Pty Ltd., (2015), Pharos-1 Well Completion Report Volume 1: Basic data, National Offshore Petroleum Information Management System (NOPIMS), Australia.

Geoscience Australia, (2022), Browse Basin regional geology, Australia.

Gawthorpe, R., Leeder, M., (2000), 'Tectono-sedimentary evolution of active extensional basins', Basin Research, vol. 12, pp. 195-218.

Grana, D., de Figureueiredo, L., Paparozzi, E. and Ravasio, A., (2025), 'Hierarchical Bayesian AVO facies inversion using Ip and Vp/Vs parameterization', Geophysics, vol. 90, no. 4, pp. M153-M165.

Handoyo, H., Ronlei, B. C., Wibowo, A. S., Fatkhan, F., Erdi, A., Avseth, P., Carbonell, R., Nugroho, P., Pandito, R. H. B., Nasibov, A., & Husein, A. A. A., (2025), Reservoir Characterization of Ngrayong Formation, Sandstone with Carbonate Intercalation, Using a Geostatistical Approach Based on Petrophysical Parameters, Northeast Java Basin, Indonesia,

Scientific Contributions Oil and Gas, vol. 48, no. 3, pp. 237-251. https://doi.org/10.29017/scog.v48i3.1828.

Haris, A., Haryono, & Riyanto, A., (2017), 'Spectral Decomposition Technique Based On Stft And Cwt for Identifying The Hydrocarbon Reservoir', Scientific contributions Oil and Gas, vol. 40, no. 3, pp. 125-131. https://doi.org/10.29017/SCOG.40.3.50.

Han, J., Lee, A., and Russell, B., (2023), 'Amplitude Versus Frequency'. GeoConvention 2023 Conference Proceedings, Calgary, Canada.

Hosseinzadeh, S., Saberi, M. R., Haghighi, M., Salmachi, A., & Salimzadeh, S., (2025), 'Seismic inversion approaches for reservoir characterization: A comprehensive review', Journal of Applied Geophysics, vol. 243, pp. 105953.

Hutabarat, P., Widarsono, B., Saptono, F., Purba, H., & Ridwan, R., (2014), Integrasi Inversi AVO dengan Model Analitik Petrofi sika untuk Menghitung Porositas dan Saturasi Air. Lembaran publikasi minyak dan gas bumi, 48 (2), 73-88. https://doi.org/10.29017/LPMGB.48.2.1216.

International Energy Agency, (2023), World Energy Outlook 2023, IEA, Paris, viewed 20 November 2025 from www.iea.org.

Kennard, J. M., Deighton, I., Ryan, D., Edwards, D. S. and Boreham, C. J., (2004), 'Subsidence and thermal history modelling: new insights into hydrocarbon expulsion from multiple petroleum systems in the Browse Basin', in Ellis, G.K., Baillie, P.W. & Munson, T.J. (eds.), Timor Sea Petroleum Geoscience: Proceedings of the Timor Sea Symposium, Darwin, Australia, 19–20 June 2003, Northern Territory Geological Survey, Special Publication, vol. 1, pp. 411–435.

Mandong, A.F., Bekti, R.P.A., & Saputra, R.I.A., (2021), Amplitude Variation with Frequency as Direct Hydrocarbon Indicator for Quick Look and Different Insight of Hydrocarbon Delineation, Jurnal Geofisika, vol. 19, no. 2, pp. 62-58.

Palu, T., Hall, L., Grosjean, E., Edwards, D., Rollet, N., Higgins, K., Boreham, C., Murray, A., Nguyen, D., Khider, K. & Buckler, T., (2017), Integrated petroleum systems analysis to understand the source of fluids in the Browse Basin, Australia, Extended abstract and poster presentation, APPEA Journal 2017, 57.

Partyka, G., Gridley, J. and Lopez, J., (1999), 'Interpretational Applications of Spectral Decomposition in Reservoir Characterization', The Leading Edge, vol. 18, pp. 353-360.

Pyrcz, M., J., Deutsch, C., V., (2014), Geostatistical Reservoir Modeling 2nd Edition, Oxford University Press, United States of America.

Setiawan, H. L., Suliantara, & Widarsono, B., (2021), Relationship Betwen Tectonic Evolutions and Presence of Heavy Oil in the Central Sumatra Basin, Scientific Contributions Oil and Gas, vol. 44, no. 1, pp. 21-37. https://doi.org/10.29017/SCOG.44.1.492.

Sinha, S., Routh, P. S., Anno, P. D., Castagna, J. P., (2005), 'Spectral Decomposition of Seismic Data with Continuous-wavelet Transform. Geophysics', Geophysic, vol. 70, no. 6, pp. 19-25.19-25.